applied sciences

MDPI

Review

A Review on Laser Powder Bed Fusion of Inconel 625 Nickel-Based Alloy

Zhihua Tian [1,2,†], Chaoqun Zhang [1,*,†], Dayong Wang [3,4], Wen Liu [5], Xiaoying Fang [6], Daniel Wellmann [1,7], Yongtao Zhao [2] and Yingtao Tian [7]

1 Shanghai Key Laboratory of Digital Manufacture for Thin-Walled Structures, School of Mechanical Engineering, Shanghai Jiao Tong University, Shanghai 200240, China; tzh4796@163.com (Z.T.); daniel.wellmann@t-online.de (D.W.)
2 School of Materials and Metallurgy, Inner Mongolia University of Science and Technology, Baotou 014010, China; zyt0011@126.com
3 State Key Laboratory of Long-Life High Temperature Materials, Dong Fang Turbine Co., Ltd., Deyang 61800, China; wangdayong@dongfang.com
4 Dongfang Electric Corporation Dongfang Turbine Co., Ltd., Deyang 618000, China
5 Department of Engineering, University of Cambridge, Cambridge CB3 0FS, UK; wl322@cam.ac.uk
6 Institute for Advanced Manufacturing, Shandong University of Technology, Zibo 255049, China; fxy@sdut.edu.cn
7 Department of Engineering, Lancaster University, Bailrigg, Lancaster LA1 4YW, UK; y.tian12@lancaster.ac.uk
* Correspondence: chaoqunzhang@sjtu.edu.cn or acezcq@gmail.com; Tel.: +86-21-3420-6543
† Zhihua Tian and Chaoqun Zhang contribute equally to this paper.

Received: 17 November 2019; Accepted: 18 December 2019; Published: 20 December 2019

Abstract: The Inconel 625 (IN625) superalloy has a high strength, excellent fatigue, and creep resistance under high-temperature and high-pressure conditions, and is one of the critical materials used for manufacturing high-temperature bearing parts of aeroengines. However, the poor workability of IN625 alloy prevents IN625 superalloy to be used in wider applications, especially in applications requiring high geometrical complexity. Laser powder bed fusion (LPBF) is a powerful additive manufacturing process which can produce metal parts with high geometrical complexity and freedom. This paper reviews the studies that have been done on LPBF of IN625 focusing on the microstructure, mechanical properties, the development of residual stresses, and the mechanism of defect formation. Mechanical properties such as microhardness, tensile properties, and fatigue properties reported by different researchers are systematically summarized and analyzed. Finally, the remaining issues and suggestions on future research on LPBF of IN625 alloy parts are put forward.

Keywords: additive manufacturing; laser powder bed fusion; Inconel 625; heat treatment; mechanical properties

1. Introduction

Additive manufacturing (AM), also known as 3D printing, is an advanced manufacturing technology developed in the past 30 years [1–3]. In theory, any CAD model created in the computer can be turned into physical objects through AM technologies, which significantly increases the freedom of geometric design and the ability to manufacture complex parts [4–10]. Laser powder bed fusion (LPBF) is one of the most promising additive manufacturing technologies for metals, which uses a high energy laser beam to melt pre-laid thin metal powder layer by layer and form high-performance parts after cooling and solidification [11–15]. Laser powder bed fusion (LPBF) is especially suitable for forming small batch, high value, customized, and complex structural parts for aerospace, biomedical, automotive, abrasive, and other applications [16–19].

Inconel 625 (IN625) is a nickel-based superalloy. It mainly draws support from the solution strengthening of some elements in the Ni–Cr matrix, such as Mo and Nb, to obtain high-temperature strength, high creep resistance. It also exhibits excellent corrosion resistance in various environments and good weldability [20–24]. However, due to its high hardness, low thermal conductivity, and high work hardening rate, IN625 is considered as an alloy difficult to machining or subtractive processing [25]. Machining tools are worn too fast and it is difficult to control the properties of IN625 in casting or forging. Therefore, new technologies are in great need for manufacturing complex-shaped IN625 parts, which are often demanded in aerospace industries.

Laser powder bed fusion (LPBF) is an emerging and powerful additive manufacturing process which is capable of producing metal parts with high geometrical complexity and freedom. As the aviation industry continuously strives to improve performance and efficiency in extreme temperatures and environments, LPBF additive manufacturing becomes a very attractive alternative solution for producing IN625 components in complex geometry [26–28]. LPBF of nickel-based alloys, including IN625 and IN718 [29–37], has been widely studied due to their high importance in aerospace industries. A detailed LPBF process schematic diagram is shown in Figure 1. LPBF is a cyclic super rapid heating and cooling process. For example, the cooling rate of the LPBF process can reach 10^6 K/s [38,39], in which the microstructure is in a non-equilibrium state and the grain growth and segregation of alloy elements are restrained accordingly [40–44]. Because of the large temperature gradient and complex heat transfer caused by laser beam cyclic processing, the microstructure and properties of the alloy tend to be anisotropic, and new metastable or even amorphous phases may be generated [45–48]. There are many variables associated with the LPBF process, such as laser power, scan speed, hatch spacing, and layer thickness. All of these variables need to be properly manipulated to successfully and reliably generate the final component, otherwise, it will result in balling, distortion, porosity, cracks, and low-density defects that seriously affect the performance of the parts [49–53]. For example, when using low laser power or high scanning speed, the molten pool is not wide enough or heated enough to combine the present track with the surrounding materials, resulting in the lack of fusion of parts [53]. In addition, the surface quality and dimensional accuracy of as-built parts are usually insufficient to meet the requirements of industrial production, so post-treatment processes such as surface processing and heat treatment are required [50,54].

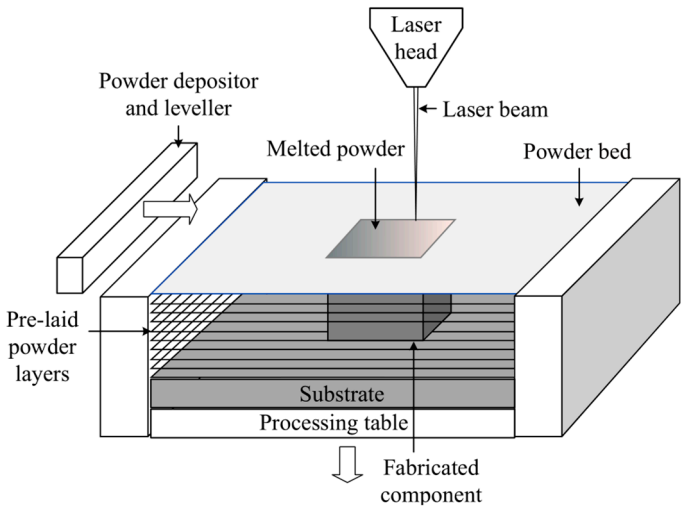

Figure 1. Schematic diagram of laser powder bed fusion (LPBF) technology [30].

Due to the key roles of Inconel 625 as a critical material used for manufacturing high-temperature bearing parts of aeroengines, the poor workability of IN625 alloy, and the difficulties to achieve high geometrical complexity using conventional manufacturing processes, it is necessary to review the current research of LPBF of Inconel 625, which provides new possibilities for manufacturing

Inconel 625 parts with high geometrical complexity and good properties. This paper reviews the studies that have been done on LPBF of IN625 focusing on the microstructure, mechanical properties, the development of residual stresses, and the mechanism of defects formation. The effects of some additional treatments (e.g., preheating, post-processing heat treatments) to relieve or eliminate residual stress inside IN625 parts undergoing LPBF and improve the quality and properties of LPBF IN625 parts were reviewed. Mechanical properties such as microhardness, tensile properties, and fatigue properties reported by different researchers are systematically summarized and analyzed. Finally, the remaining issues and suggestions on future research on LPBF of IN625 alloy parts are put forward.

2. Macroscopic Characteristics of Samples

The surface morphology of LPBF parts is related to the laser scanning process. In the work conducted by Li et al. [55], the surface of the as-built IN625 sample presented a typical "V" shape morphology (Figure 2a), which is similar to the situation in the welding process. However, the shape of the Y–Z section is "scales" as shown in Figure 2b. The width of the melt track is about 100 μm, and the adjacent tracks overlap closely, resulting in nearly 100% density and almost no gaps. The "V" angle increases as the laser scanning speed decreases.

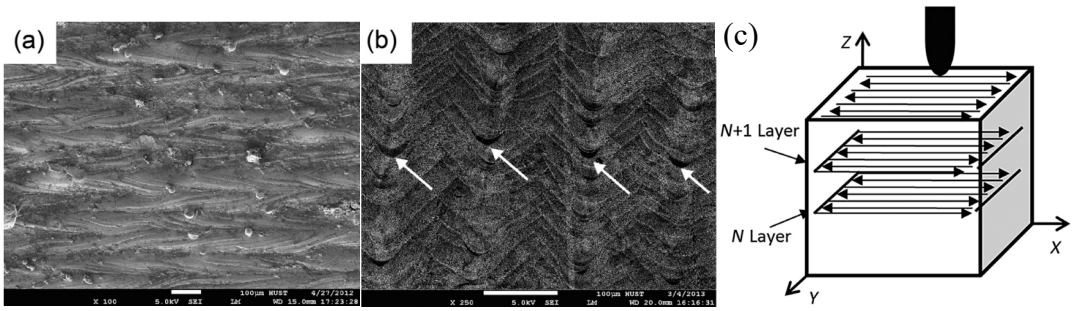

Figure 2. Macroscopic morphology characteristics of as-built Inconel 625 (IN625) samples: (**a**) top surface morphology, (**b**) "scales" shape of Y-Z section, and (**c**) illustration of the coordinate system and laser scanning mode [55].

Mumtaz et al. [30,56] used LPBF pulse shaping IN625 alloy to study the effect of process parameters on the roughness (R_a) of top and side of thin-walled parts and prepared the best sample with 9 μm roughness on the top surface and 10 μm roughness on the side face. They concluded that higher peak power could reduce balling formation by increasing melt wettability, thereby reducing the top and side R_a. Large laser repetition rate, low scanning speed, high spot overlap rate, and high energy density decrease the top R_a but increase the side R_a. By controlling these factors reasonably, low R_a on the top surface and side can be obtained simultaneously [56,57].

By melting the IN625 bare plate, the melt pool geometry (width and depth) of IN625 alloy during LPBF process can be capably reflected, in which typical chevron features (Figure 3) of solidified materials appear due to fluid flow and free surface evolution [58]. Specifically, the increase of scanning speed leads to an increase of chevron spacing, but the angle of the chevrons decreases. To eliminate the thermal stress concentration caused by the chevron feature of LPBF sample surfaces, Yang et al. [59] used M280 laser forming equipment to print the IN625 metallographic sample, and the laser scanning path was superposed with different angles. Although a few irregular microcracks appear on the sample surface, there is no obvious transition region between the laser beam action region, and the single track melting layer perpendicular to the scanning direction of the laser beam shows an arc distribution.

Overall, IN625 has good LPBF forming ability with a wide limit range of process parameters [60]. High density (e.g., 99.99% [61] and 99.74% [62]) and smooth surfaces can be obtained by carefully controlling the processing parameters. The macroscopic characteristics of the as-built IN625 samples are closely related to the process parameters. It is obvious that the chevron feature of the track can be seen in almost all previous studies [55–62].

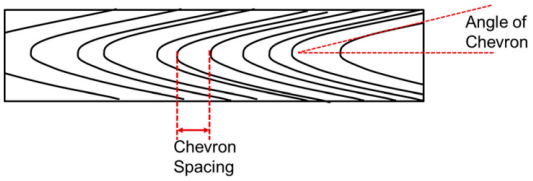

Figure 3. Schematic diagram of typical chevron features on the surface of the as-built IN625 sample [58].

3. Microstructure

3.1. Microstructure in As-Built State

Similar to the grain growth behavior in most LPBF alloys, as-built IN625 consists of some cellular dendrites and columnar grains with elongated grains in the building direction (see Figure 4) [49]. To be more specific, LPBF IN625 alloy has a typical gamma face-centered cubic (γ-FCC) matrix and a strong texture with <100> orientations parallel to the Z-axis direction [55]. Due to factors such as heterogeneous nucleation of the impurity elements and heat dissipation disorder at the boundary of the molten pool, some non <100> oriented grains also can undergo restricted growth, resulting in many fine grains. In the center of the molten pool, the size of the grains is relatively large and the orientation is more uniform. Moreover, precipitations like γ', γ'' phases, Laves phase, and some MC carbide are often observed in the as-built state. The presence of intergranular brittle Laves lead to the mechanical properties and creep properties of the direct LPBF parts much lower than the standards of aerospace forgings. Amato et al. [63] also observed an intermetallic strengthening precipitate γ' (Ni_3Nb) positioned along the boundary of the molten pool. Yang et al. [59] observed single austenite with large lattice distortion but no carbides and precipitates in the as-built IN625 alloy. In addition, element segregation and extremely high dislocation density exist in individual grains as well as in the whole component [50].

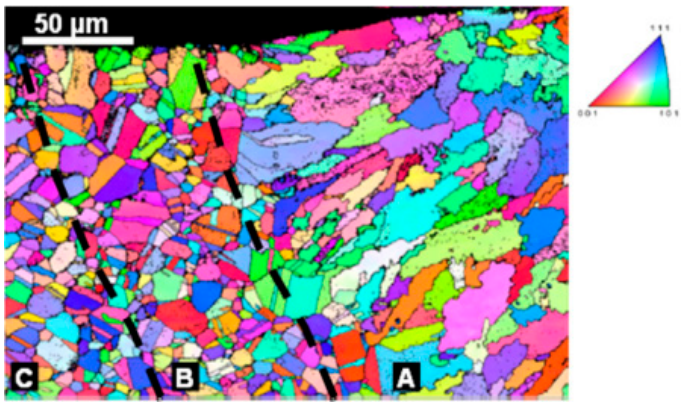

Figure 4. Inverse pole figure of the cross-section of the as-built IN625 track. A represents the track, B represents the heat-affected zone, and C represents the substrate [49].

The process parameters of the LPBF, as well as the powder factor, will have a significant impact on the microstructure of the formed part. Li et al. [49] conducted a single track LPBF of IN625 experiment and found that the effect of laser power on the spacing of primary cells is greater than the effect from scanning speed. With the increase of laser power and the decrease of scanning speed, the track width, and melt depth increased, and the contact angle of the melt pool decreased with the increase of power, while the height and surface roughness of the melt pool had nothing to do with the scanning speed, which was consistent with the research results of Mumtaz et al. [30]. According to Li Shuai's research [64], the laser scanning direction is also related to the texture characteristics of the LPBF of the IN625 alloy. When the bi-directional scanning is carried out, the grains all extend along the direction of <100>, while the grain growth direction forms an angle of 60° with the forming direction

when adopting unidirectional scanning, which is mainly caused by the asymmetry between heat flow direction and printing direction.

As discussed in the work conducted by Yang et al. [59], the microstructure of the as-built IN625 alloy sample is uniform and fine, showing obvious rapid solidification characteristics. The sample consists of a single austenite phase, and some carbon–oxygen inclusions are present inside. Using EBSD, Li Shuai et al. [55] reported that the texture was stronger under the condition of higher power when comparing 1000 W to 400 W. In summary, the main phase in as-built LPBF IN625 samples is Ni-matrix. Sometimes carbides and some second phases precipitated [63], sometimes they were not observed [59], which is mainly related to the process parameters. High laser power and slow laser scanning speed lead to more laser heat input, which increases the penetration and the width of the weld bead [30,49] and also enhances the texture [55]. More studies on the correlation between LPBP processing parameters and the as-built microstructures are needed for a deeper understanding of the microstructure evolutions during LPBF and precisely achieving the desired microstructures.

3.2. Microstructure After Heat Treatments

To eliminate or ameliorate the non-equilibrium phase, the Laves phase, and the micro-cracks existing inside the alloy after LPBF manufacturing, and the residual internal stress of the macro part, it is often necessary to perform a suitable heat treatment process on the as-built part. In general, there are mainly four types of post-treatments recommended for the LPBF of IN625: stress relief annealing, recrystallization annealing, solution treatment, and hot isostatic pressing [65,66]. Li et al. [55] carried out heat treatment on as-built IN625 samples by heating them to 700 °C, 1000 °C, and 1150 °C and holding for one hour before air cooling. It was found that the microstructure of IN625 parts at the condition of annealing at 700 °C was the same as that of an as-built state. When annealed at 1000 °C, solute elements were homogenized and some fine grains were formed. The original molten pool boundary gradually disappeared and a lot of MC carbides were precipitated at the grain boundary. At 1150 °C, the grains grew significantly, and the carbides at the grain boundaries still existed and coarsened. Because of heat conduction in the LPBF process, most grains had obvious preferential orientation after heat treatment. Comparison of different annealing temperatures [50,55], one can conclude that high-temperature annealing enables recrystallization (Figure 5a) of as-built IN625 sample, high Z-contrast precipitates are dissolved and MC carbides precipitate, and the grain boundaries become serration due to the pinning effect from MC carbides (Figure 5b).

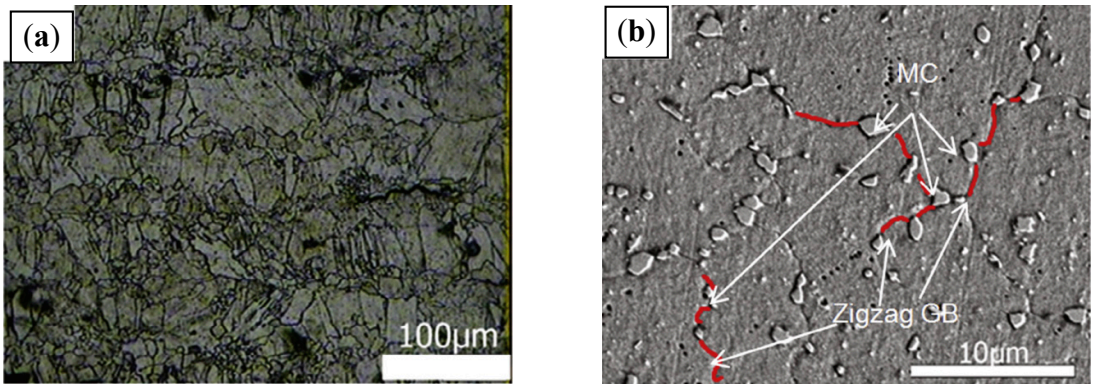

Figure 5. X–Y plane microstructure of the LPBF of IN625 samples after annealing at 1150 °C. (**a**) Optical metallographic image, (**b**) grain boundary structure, and the carbides distribution [55].

Fang et al. [65] focused on the effect of annealing temperature on texture and grain boundary character distribution of as-built samples. After recovery annealing at 870 °C and 980 °C, the weak texture similar to the cube-oriented type can be observed. While conducting recrystallization annealing at 1500 °C, a strong {110} <01-1> (X–Y plane) texture appears. The fraction of low angle grain boundary

in the as-built sample was significantly reduced, concomitantly many $\sum 3^n$ grain boundaries and some $\sum 3^n$ grain clusters were generated. The {110} type texture instead of cube-oriented texture is beneficial for multiple twining, which can be used for grain boundary character distribution optimization. The study of Dinda et al. [60] showed that the dendrite structure of as-built IN625 was maintained when it was annealed below 1000 °C, and some new grains appeared at the interface between the deposition layer and the substrate, while some of them were recrystallized when it was annealed at 1100 °C. At 1200 °C, complete recrystallization occurred, and the grains became equiaxed and a large number of annealing twins appeared to release residual stress.

In summary, the desired microstructure evolutions occurred when the annealing temperature is above 1000 °C [55,60]. Below 1000 °C, no obvious microstructure evolution was observed. High-temperature annealing heat treatments above 1000 °C are accompanied by the obvious occurrence of recrystallization and the release of residual stress [60]. In the range of medium temperature (several hundred °C to 1000 °C), the microstructure of IN625 almost did not change, which shows that the IN625 parts formed by LPBF have a high thermal stability [60]. More studies on the influence of various heat treatments on the microstructure evolution and residual stress release are necessary to better control the properties of LPBF IN625 parts through low-cost and highly efficient heat treatments.

4. Residual Stresses and Distortion

During LPBF, a steep thermal gradient certainly exists between the melt pool and the relatively cold substrate (or previously consolidated layer), resulting in high residual stress inside the LPBF parts [65,67]. The accumulated residual stress will lead to distortion, geometric failure and even crack. Therefore, it is very important to study the residual stress level in IN625 alloy parts produced by LPBF. When directly printing the IN625 alloy tensile samples by LPBF [59], the residual stresses on the surface of the samples before and after annealing were all in tension. Before annealing, the residual stresses on the sample surface fluctuate considerably due to the different cooling conditions at different locations during laser forming, with an average value of 398 MPa [59]. After annealing, the average residual stress was 242 MPa, which is still at a considerably high level. To relieve the residual stress, Zhang et al. [68] preheated the LPBF substrate at 20 °C (room temperature), 150 °C, and 300 °C, and found that the residual stress decreased with the increase of preheating temperature. When the preheating temperature reached 300 °C, the residual stress (160.7 MPa) of the LPBF of IN625 alloy decreased by more than 50% compared with that without preheating. The residual stress increases with the increase of the temperature gradient. When the substrate is preheated, the heat input of laser can be greatly reduced, thereby reducing the temperature gradient; besides, preheating reduces the yield strength of the material, so the maximum residual stress can be reduced [69]. Fang et al. [65] show that for the LPBF IN625 shaped specimens, the residual stress inside the specimen is still high even after annealing at 980 °C and subsequent two-step stress relief annealing of 16 h. However, when the annealing temperature reaches 1150 °C, the low angle grain boundaries and internal residual stress (local deformation), which is the driving force for recrystallization can be clearly eliminated. Similar results were obtained by Li et al. [50] and Kreitcberg et al. [66]. Based on the above studies, we can reach a conclusion that residual stress can only be significantly eliminated by very-high-temperature heat treatments.

In addition, distortion often occurs in LPBF formed IN625 alloy parts, as described in Figure 6. Leary et al. [70] prepared IN625 lattice structures using LPBF, and some geometric distortion (Figure 6a) and visible oxidation would occur to the strut with a larger diameter. Distortion and roughness were easily observed on the downward-facing surfaces. An even higher heat input was used by Li et al. [49] under a laser power of 60 W and a scanning speed of 1500 mm/min. In this instance, the single track IN625 alloy fabricated by LPBF showed irregularity and distortion (Figure 6b) due to the decrease in viscosity of the molten metal and increased vapor recoil force. Whereas according to the discussion of Balbaa et al. [67], there was no clear trend of influence of process parameters on surface residual stresses in LPBF IN625 parts.

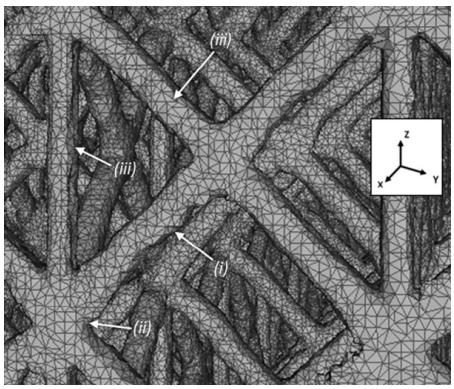

(**a**)

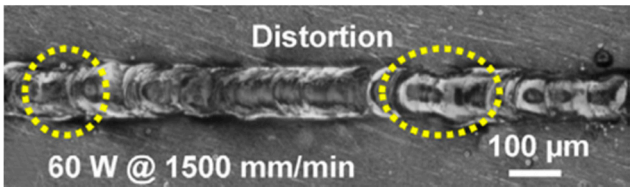

(**b**)

Figure 6. Distortion of the LPBF IN625 alloy. (**a**) Distortion in the lattice structure [70]; (**b**) distortion in the single track [49].

5. Defects

While forming a unique microstructure, the LPBF process may also induce metallurgical defects, such as pores, inclusions, cracks and poor interlayer fusion due to improper control of the forming process, which may further affect the mechanical properties of the fabricated parts. Common metallurgical defects of IN625 formed parts obtained by the LPBF process are summarized in Table 1. As Li et al. [50] mentioned, the apparent porosity and balling spheres are the main reasons for the poor surface finish of as-built IN625 alloy samples. When macroscopic defects occur in the LPBF sample, microscopic defects also increase. The density of parts is mainly related to the selection of processing parameters [49,70]. When the forming quality of the specimen is good, the defects mainly consist of tiny holes or few cracks, and most of them exist on the surface or subsurface layer of the specimen. The size of holes can be reduced by preheating the substrate [68] or conducting stress relief annealing [59], etc. Poulin et al. [62] produced up to 10% porosity in LPBF IN625 samples by intentionally seeding pores by changing the laser scanning speed to study the influence of porosity on long fatigue crack propagation behavior. By increasing the scanning speeds from 960 mm/s to 1920 mm/s (960, 1440, 1680, and 1920 mm/s), the intentionally-seeded porosities increased from 0.1% to 2.7% (0.1, 0.3, 0.9, and 2.7%). It can be seen that the relation between scanning speeds and porosities is not linear and the porosities boomed when the scanning speed exceeded a certain value.

Overall, using appropriate process parameters, preheating the substrate, and conducting stress relief annealing are effective measures to reduce defects in LPBF parts.

Table 1. Main defects and formation reasons of LPBF IN625 alloy parts.

Density	Defects	Formation Reasons	Elimination (Weakening) Measures	Ref.
Almost 100%	A lack of fusion, gas entrapment porosity	Powder factor	Reasonable process parameters	[45]
–	Macro defect: balling, irregularity, distortion, spatter, un-melted particles, necking micro defect: unmelted, inclusions, cracks, porosity (20~100 μm)	Insufficient heat input, low melt viscosity, instability of melt pool	Reasonable process parameters	[49]
–	Surface topography: open pore, balling, micro-cracks subsurface defect: pores	Uneven layer thickness distribution, high tensile residual stress, high viscosity and surface tension of the melt pool material	–	[50]
–	Surface cracks, internal inclusions	Oxidation, residual thermal stress	Annealing	[59]
99%	Surface cracks	Local eutectic structure (γ + Laves), residual thermal stress	Substrate preheating	[68]
Related to laser parameters	Most pores and a small number of cracks in inter-layer boundaries	–	–	[71]

6. Mechanical Properties

6.1. Hardness Distribution

In general, hardness is positively related to the tensile strength of the material and higher hardness means higher strength of the material. Therefore, measuring the hardness of the LPBF samples can provide some references for the strength of the samples. The LPBF IN625 alloy has a large degree of anisotropy in hardness produced by typical anisotropic microstructure, and the plane perpendicular to the building direction exhibits higher hardness due to the higher concentration of the barriers to dislocation under the surface [45,66]. Zhang et al. [71] studied the effects of laser energy density (LED) on the microhardness of LPBF IN625 samples. It was found that when the LED was increased from 400 J/m to 1200 J/m, the microhardness increased from 300 to 350 $HV_{0.3}$, but the increase was not very large. However, when 5 wt% of TiB_2 particles were added to the original powder, the hardness of the IN625 formed part was significantly improved due to the change in microstructure. When the LED was increased from 400 J/m to 1200 J/m, the microhardness was increased from 600 to 700 $HV_{0.3}$. The maximum average microhardness (293 HBW) of the LPBF IN625 sample with the lowest porosity (0.036%) was obtained by Marchese et al. [72] at a scanning speed of 900 mm/s with a laser power of 175 W and a hatching distance of 0.07 mm values. They also pointed out that the reduction of hatching distance can improve the density and hardness of the part, while high scanning speed had the opposite effect. To obtain a hardness suitable for the working environment, many researchers have also studied the influence of heat treatment and second phase particles on the hardness of LPBF IN625 parts. Li et al. [55] studied the relationship between annealing temperature and hardness of LPBF IN625 samples. Due to the very fine structure and the solid solution strengthening effect of many solute elements, the average hardness of as-built IN625 samples was very high (343 HV), which was even higher than the 305 HV obtained by the traditional forging process. When the annealing temperature was 700 °C, the hardness of the sample decreased due to the relaxation of residual stress. When the annealing temperature was 800 °C and 900 °C, the hardness increased due to the precipitates of the δ phase (Ni_3Nb) in the annealing process. Above 1000 °C, the δ phase was dissolved in the Ni matrix, so the hardness decreased rapidly. Wong et al. [61] printed IN625 alloy using the multi-laser method and found that the average hardness (284.25 $HV_{0.5}$) and grain size (10–100 μm) of the samples obtained were the same as those reported in the literature (280 $HV_{0.5}$ [73]) by a single laser. They also found that heat treatment could reduce the hardness (271.08 $HV_{0.5}$).

In the work conducted by Li et al. [49], the hardness of the LPBF IN625 sample did not have any tendency in the depth direction, and the hardness of the track was higher than that of HAZ. They also found that the heat-treated sample can show a lower microhardness value than the as-built sample [50]. Similar results were obtained by Balbaa et al. [67], although the microhardness measured in the build (Z) direction changed with the increase in laser power, the change was not significant when considering

standard deviation and microstructure. However, the effect of hatch spacing increase on part hardness was not monotone. The maximum hardness was always obtained near the top surface.

6.2. Tensile Strength

As mentioned above, the IN625 alloy directly formed by the LPBF process consists mainly of a large number of fine γ phases. Therefore, the hardness and corresponding strength of LPBF parts are higher than those prepared by conventional techniques [67]. However, because of the forming characteristics of LPBF, there is large residual stress inside the parts. The plasticity index of LPBF shaped parts without any subsequent treatment is usually difficult to reach the commonly used casting and forging standards. Due to the directional solidification characteristics, there are typical textures that existed in LPBF IN625 alloy parts, which leads to the anisotropy of mechanical properties of the alloy. Thus, not only the hardness but also the tensile properties vary in different directions. The post-treatment can decrease the microstructure anisotropy of the LPBF IN625 alloy and have a significant impact on the mechanical properties. The strength and plasticity of as-built and heat-treated IN625 alloys are shown in Table 2.

Table 2. Mechanical properties of LPBF IN625 alloys from different literature.

Materials	Condition	Yield Strength (mpa)	Ultimate Tensile Strength (mpa)	Elongation (%)	Reduction of Area (%)	Ref.
IN625	As-built	743	1043	31.4	49.6	[59]
IN625	LPBF+annealing	386	910	54.4	56.6	[59]
IN625	As-built (multi-laser)	585	864	58.6	–	[61]
IN625	As-built (multi-laser) + heat treatment	507	827	69.3	–	[61]
IN625	As-built	641.5	878.5	30	–	[74]
MWCNT-IN625	As-built	788	998	19.1	–	[74]
MWCNT-IN625	LPBF + heat treatment	585	1000	31.5	–	[74]
IN625	Wrought	517	930	40	–	[75]

As can be seen from Table 2, the strength of LPBF IN625 alloy parts is generally higher than the wrought part. Although adopting the multi-laser method to increase the construction efficiency, the mechanical properties of the LPBF samples are still comparable with a single laser method and heat treatment at 1048 °C for 1 h can reduce the strength of the multi-laser specimen and improve the plasticity to a certain extent [61]. The average yield strength and tensile strength of as-built parts obtained by Wang et al. [74] are lower than those by Yang et al. [59], and the elongation after fracture is similar. To one's delight, their tensile properties are similar to those of traditional forged IN625 alloy [75], which is much higher than the minimum tensile properties specified by ASTM B446-03. After annealing [59], the average yield strength decreases, but the tensile strength does not change much. After adding 0.5 wt% multi-wall carbon nanotube (MWCNT), the strength of the IN625 alloy in as-built state increased significantly, but the plasticity also deteriorated accordingly [74]. After solution treatment at 1040 °C for 2 h and two-step aging treatment (720 °C for 7 h and 650 °C for 8 h), the strength of MWCNT-IN625 decreased to a certain extent, but the plasticity was restored, which indicates that it is feasible to achieve the coordination of strength and plasticity of LPBF IN625 parts by heat treatment [74]. According to the research of Yadroitsev et al. [75] when the angle between the laser scanning direction and the growth direction of the columnar crystal is changed (0°, 45°, 90°), the tensile properties of "horizontal" and "vertical" samples are almost the same, indicating that mechanical properties will not be affected by the scanning strategy. In addition, the study of Inaekyan et al. [76] shows that the δ phase precipitated in the process of stress relief annealing at 870 °C and the carbide precipitated in the solution treatment at 1120 °C did not cause the high-temperature plastic loss of LPBF IN625 alloy, mainly because of that the deformation of the solution treated alloy at high-temperature is accompanied by dynamic strain aging, while the deformation after stress relief and medium temperature annealing are accompanied by dynamic recrystallization. Therefore, there is a competition between dynamic strain aging and dynamic recrystallization at high-temperature. The former decreases the plasticity while the latter increases the plasticity of the alloy.

In summary, the typical textures that existed in LPBF IN625 alloy parts leads to the anisotropy of tensile strength and other mechanical properties. Heat treatments can significantly change the tensile strength and increase the ductility of LPBF IN625 alloy samples [59,61,74]. The significant strengthening effect of adding carbon nanotube into IN625 [74] indicates that adding second tiny strengthening phases could be a useful method to improve the mechanical properties of LPBF IN625. When using the highly efficient multi-laser LPBF to produce IN625 samples, the mechanical properties of the samples are still comparable with those produced by a conventional single laser method [61].

6.3. Other Properties

At present, there are few reports on other important properties of LPBF IN625 alloy parts, such as high-temperature tensile strength, corrosion resistance and creep properties. The study by Tascioglu et al. [54] showed that the wear rate of LPBF IN625 parts could be reduced by 50% by implementing mechanical post-treatment operation (milling). By reducing the feed speed, the surface quality can be improved and the influence of machining on the surface of parts can be reduced. When building from two different directions of 45 mm × 20 mm × 4 mm IN625 rectangular samples [75], there were a large number of defects in "vertical" samples causing by more layers and a larger amount of thermal stress accumulation during the LPBF forming process, the young's modulus value of the "horizontal" sample was about 1.5 times higher than that of the "vertical" samples, and it was close to 207 MPa of the wrought IN625. Koutiri et al. [77] performed fatigue tests on both as-built and polished samples and found that, although the polished sample had a lower surface roughness, the fatigue strength was similar in both cases because they all contained similar size/population of defects leading to cracking. In addition, Poulin et al. [62] reported that the intentionally-seeded porosity of 0.1, 0.3, 0.9 and 2.7% in samples had very limited influence on the near threshold fatigue crack growth behavior of LPBF IN625 alloy. Overall, there is a great need for the carrying out of the damage tolerance approach for the design and quality control of LPBF IN625 parts [62].

7. Summary and Outlook

As an important type of additive manufacturing technologies, LPBF offers great potential for the production of complex components. The current studies on LPBF of IN625 mainly focus on regulating the microstructure and properties by changing LPBF process parameters and subsequent heat treatment. As the LPBF process involving complex problems such as metallurgy, physics, chemistry and thermal coupling, and the matching relationship between process parameters is very complex, so the currently available parameters for LPBF of IN625 are yet immature and insufficient. A high level of residual stress often exists in the specimens and causes cracking. Other defects, such as holes, cracks, and inclusions often appear between the layers. The performance anisotropy of the sample often arises due to the presence of texture in the LPBF IN625 alloy, but sometimes it is not desirable to have a larger performance difference between forming planes. Moreover, the non-equilibrium solidification results in a significant increase in the solution limit of alloying elements in matrix metals, which makes the performance of LPBF parts different from that of the conventional bulk material. To date, most of the studies on LPBF of IN625 focus on micro-hardness and tensile properties, and there are few studies done on other important properties such as high-temperature tensile strength, corrosion resistance, and creep properties. Consequently, future studies should focus on the following aspects:

(1) Characterize the macroscopic defects and microstructure of as-built and post-treated IN625 alloy to deeply explore the formation mechanism of macroscopic defects (pores, microcracks, balling, un-melted zone) and the microstructure evolution mechanism (grain boundary, second-phase, dislocation, subgrain boundary, stacking fault, etc.).

(2) Study the anisotropy and site-specific features of high and low-temperature performance (strength, fatigue, creep, corrosion, etc.) of LPBF IN625 alloy and clarify the reasons, especially the influence of macro anisotropy and microstructure anisotropy at the as-built and post-treated states on the above-mentioned properties.

(3) Establish models to predict the microstructure evolution and residual stress distribution of LPBF IN625 alloy, i.e., building the relationship between LPBF parameters, microstructure, residual stress, and mechanical properties.

Author Contributions: Z.T. and C.Z. contribute equally to this paper. Writing—original draft, Z.T.; writing—outline of the paper, review and editing, supervision, funding acquisition, C.Z.; review and editing, D.W., W.L., X.F., Y.T. All authors have read and agreed to the published version of the manuscript.

Funding: This work was supported by the National Natural Science Foundation of China, grant number 51605287, and Natural Science Foundation of Shanghai, grant number 16ZR1417100. This work was also supported by the fund of State Key Laboratory of Long-Life High Temperature Materials.

Acknowledgments: We appreciate the help from Xiqian Wang (University of Birmingham, Oerlikon) and Zhenbo Zhang (University of Manchester) for the useful discussion.

Conflicts of Interest: The authors declare no conflict of interest.

References

1. Lu, B.H.; Li, D.C. Development of the additive manufacturing (3D printing) technology. *Mach. Build. Autom.* **2013**, *42*, 1–4.
2. Huang, Y.; Leu, M.C.; Mazumder, J.; Donmez, A. Additive Manufacturing: current state, future potential, gaps and needs, and recommendations. *J. Manuf. Sci. Eng.* **2015**, *137*, 014001. [CrossRef]
3. Li, H.L.; Jia, D.C.; Yang, Z.H.; Duan, X.M.; Cai, D.L.; Zhou, Y. Research progress on selective laser melting 3D printing of titanium alloys and titanium matrix composites. *Mater. Sci. Technol.* **2019**, *27*, 1–15.
4. Chen, L.; He, Y.; Yang, Y.X.; Ren, H.T. The research status and development trend of additive manufacturing technology. *Int. J. Adv. Manuf. Technol.* **2016**, *89*, 3651–3660. [CrossRef]
5. Gibson, I.; Rosen, D.; Stucker, B. *Additive Manufacturing Technologies: 3D Printing, Rapid Prototyping, and Direct Digital Manufacturing*; Springer: New York, NY, USA, 2010; ISBN 978-1-4939-2112-6.
6. Erhard, B.; Ulrike, H.; Vitus, H.; Damien, B. Additive manufactured AlSi10Mg samples using selective laser melting (SLM): microstructure, high cycle fatigue, and fracture behavior. *Mater. Des.* **2012**, *34*, 159–169.
7. Zhang, B.C.; Liao, H.L.; Christian, C. Effects of processing parameters on properties of selective laser melting Mg–9%Al powder mixture. *Mater. Des.* **2012**, *34*, 753–758. [CrossRef]
8. Vaezi, M.; Seitz, H.; Yang, S.F. A review on 3D micro-additive manufacturing technologies. *Int. J. Adv. Manuf. Tech.* **2013**, *67*, 1721–1754. [CrossRef]
9. Poulin, J.R.; Brailovski, V.; Terriault, P. Long fatigue crack propagation behavior of Inconel 625 processed by laser powder bed fusion: influence of build orientation and post-processing conditions. *Int. J. Fatigue* **2018**, *116*, 364–647. [CrossRef]
10. Gao, W.; Zhang, Y.B.; Ramanujan, D.; Ramani, K.; Chen, Y. The status, challenges, and future of additive manufacturing in engineering. *Comput. Aided Des.* **2015**, *69*, 65–89. [CrossRef]
11. Rochus, P.; Plesseria, J.Y.; Elsen, M.V.; Kruth, J.P.; Carrus, R.; Dormal, T. New applications of rapid prototyping and rapid manufacturing (RP/RM) technologies for space instrumentation. *Acta Astronaut.* **2007**, *61*, 352–359. [CrossRef]
12. Criales, L.E.; Arısoy, Y.M.; Özel, T. Sensitivity analysis of material and process parameters in finite element modeling of selective laser melting of Inconel 625. *Int. J. Adv. Manuf. Tech.* **2016**, *86*, 2653–2666. [CrossRef]
13. Rashid, R.; Masood, S.H.; Ruan, D.; Palanisamy, S.; Rahman Rashid, R.A.; Brandt, M. Effect of scan strategy on density and metallurgical properties of 17-4PH parts printed by Selective Laser Melting (SLM). *J. Mater. Sci. Technol.* **2017**, *249*, 502–511. [CrossRef]
14. Zhang, J.L.; Song, B.; Wei, Q.S.; Bourell, D.; Shi, Y.S. A review of selective laser melting of aluminum alloys: processing, microstructure, property and developing trends. *J. Mater. Sci. Technol.* **2019**, *35*, 270–284. [CrossRef]
15. Kruth, J.P.; Levy, G.; Klocke, F.; Childs, T.H. Consolidation phenomena in laser and powder-bed based layered manufacturing. *CIRP Ann.* **2007**, *56*, 730–759. [CrossRef]
16. Frazier, W.E. Metal additive manufacturing: A review. *J. Mater. Eng. Perform.* **2014**, *23*, 1917–1928. [CrossRef]
17. Clare, A.T.; Chalker, P.R.; Davies, S.; Sutcliffe, C.J.; Tsopanos, S. Selective laser melting of high aspect ratio 3D nickel–titanium structures two way trained for MEMS applications. *Int. J. Mech. Mater. Des.* **2008**, *4*, 181–187. [CrossRef]

18. DebRoy, T.; Wei, H.L.; Zuback, J.S.; Mukherjee, T.; Elmer, J.W.; Milewski, J.O.; Beese, A.M.; Wilson-Heid, A.; De, A.; Zhang, W. Additive manufacturing of metallic components-Process, structure and properties. *Prog. Mater. Sci.* **2018**, *92*, 112–224. [CrossRef]
19. Wang, X.; Carter, L.N.; Pang, B.; Attallah, M.M.; Loretto, M.H. Microstructure and yield strength of SLM-fabricated CM247LC Ni-Superalloy. *Acta Mater.* **2017**, *128*, 87–95. [CrossRef]
20. Xu, F.J.; Lv, Y.H.; Liu, Y.X.; Shu, F.Y.; He, P.; Xu, B.S. Microstructural evolution and mechanical properties of Inconel 625 alloy during pulsed plasma arc deposition process. *J. Mater. Sci. Technol.* **2013**, *29*, 480–488. [CrossRef]
21. Ramkumar, K.D.; Abraham, W.S.; Viyash, V.; Arivazhagan, N.; Rabel, A.M. Investigations on the microstructure, tensile strength and high temperature corrosion behaviour of Inconel 625 and Inconel 718 dissimilar joints. *J. Manuf. Process.* **2017**, *25*, 306–322. [CrossRef]
22. Pavithra, E.; Senthil Kumar, V.S. Microstructural evolution of hydroformed Inconel 625 bellows. *J. Alloy. Compd.* **2016**, *669*, 199–204. [CrossRef]
23. Shoemaker, L.E. Alloys 625 and 725: trends in properties and applications. *Superalloys* **2005**, *718*, 625–706.
24. Ozgun, O.; Gulsoy, H.O.; Yilmaz, R.; Findik, F. Injection molding of nickel based 625 superalloy: Sintering, heat treatment, microstructure and mechanical properties. *J. Alloy. Compd.* **2013**, *546*, 192. [CrossRef]
25. Nath, C.; Brooks, Z.; Kurfess, T.R. On Machinability study and process optimization in face milling of some alloys with indexable copy face mill inserts. *Procedia Manuf.* **2015**, *1*, 487–500. [CrossRef]
26. Mohammadian, N.; Turenne, S.; Brailovski, V. Surface finish control of additively–manufactured Inconel 625 components using combined chemical–abrasive flow polishing. *J. Mater. Process. Technol.* **2018**, *252*, 728–738. [CrossRef]
27. Gonzalez, J.A.; Mireles, J.; Stafford, S.W.; Perez, M.A.; Terrazas, C.A.; Wicker, R.B. Characterization of Inconel 625 fabricated using powder-bed-based additive manufacturing technologies. *J. Mater. Process. Tech.* **2019**, *264*, 200–210. [CrossRef]
28. Amato, K.N.; Gaytan, S.M.; Murr, L.E.; Martinez, E.; Shindo, P.W.; Hernandez, J.; Collins, S.; Medina, F. Microstructures and mechanical behavior of Inconel 718 fabricated by selective laser melting. *Acta Mater.* **2012**, *60*, 2229–2239. [CrossRef]
29. Wang, Z.; Guan, K.; Gao, M.; Li, X.Y.; Chen, X.F.; Zeng, X.Y. The microstructure and mechanical properties of deposited–IN718 by selective laser melting. *J. Alloy. Compd.* **2012**, *513*, 518–523. [CrossRef]
30. Mumtaz, K.; Hopkinson, N. Selective laser melting of Inconel 625 using pulse shaping. *Rapid Prototyp. J.* **2010**, *16*, 248–257. [CrossRef]
31. Jia, Q.B.; Gu, D.D. Selective laser melting additive manufacturing of inconel 718 superalloy parts: Densification, microstructure and properties. *J. Alloy. Compd.* **2014**, *585*, 713–721. [CrossRef]
32. Zuo, W.; Zhang, Q.M.; Wu, W.J.; Zhou, H.G. Microstructure of selective laser melted nickel-based superalloy K4202. *J. Rocket Propuls.* **2017**, *43*, 55–59.
33. Tomus, D.; Rometsch, P.A.; Heilmaier, M.; Wu, X.H. Effect of minor alloying elements on crack-formation characteristics of Hastelloy-X manufactured by selective laser melting. *Addit. Manuf.* **2017**, *16*, 65–72. [CrossRef]
34. Cloots, M.; Uggowitzer, P.J.; Wegener, K. Investigations on the microstructure and crack formation of IN738LC samples processed by selective laser melting using gaussian and doughnut profiles. *Mater. Des.* **2016**, *89*, 770–784. [CrossRef]
35. Rickenbacher, L.; Etter, T.; Hövel, S.; Wegener, K. High temperature material properties of IN738LC processed by selective laser melting (SLM) technology. *Rapid Prototyp. J.* **2013**, *19*, 282–290. [CrossRef]
36. Kanagarajah, P.; Brenne, F.; Niendorf, T.; Brenne, F.; Maier, H.J. Inconel 939 processed by selective laser melting: effect of microstructure and temperature on the mechanical properties under static and cyclic loading. *Mater. Sci. Eng. A* **2013**, *588*, 188–195. [CrossRef]
37. Popovich, V.A.; Borisov, E.V.; Popovich, A.A. Impact of heat treatment on mechanical behaviour of Inconel 718 processed with tailored microstructure by selective laser melting. *Mater. Des.* **2017**, *131*, 12–22. [CrossRef]
38. Paul, C.P.; Ganesh, P.; Mishra, S.K.; Bhargavaa, P.; Negib, J.; Natha, A.K. Investigating laser manufacturing for Inconel-625 components. *Opt. Laser Technol.* **2007**, *39*, 800. [CrossRef]
39. Thijs, L.; Sistiaga, M.; Wauthle, R.; Xie, Q.; Kruth, J.; Humbeeckl, J. Strong morphological and crystallographic texture and resulting yield strength anisotropy in selective laser melted tantalum. *Acta Mater.* **2013**, *61*, 4657–4668. [CrossRef]

40. Vilaro, T.; Colin, C.; Bartout, J.D.; Nazéb, L.; Sennourb, M. Microstructural and mechanical approaches of the selective laser melting process applied to a nickel-base superalloy. *Mater. Sci. Eng. A* **2012**, *534*, 446–451. [CrossRef]
41. Li, Y.; Gu, D. Parametric analysis of thermal behaviour during selective laser melting additive manufacturing of aluminium alloy powder. *Mater. Des.* **2014**, *63*, 856–867. [CrossRef]
42. Fu, C.; Guo, Y. Three-dimensional temperature gradient mechanism in selective laser melting of Ti-6Al-4V. *J. Manuf. Sci. Eng.* **2014**, *136*, 061004. [CrossRef]
43. Wang, X.B.; Sergey, K.; Humbeeck, J.V. A short review on the microstructure, transformation behavior and functional properties of NiTi shape memory alloys fabricated by selective laser melting. *Materials* **2018**, *11*, 1683. [CrossRef] [PubMed]
44. Zhang, Y.N.; Cao, X.; Wanjara, P. Microstructure and hardness of fiber laser deposited Inconel 718 using filler wire. *Int. J. Adv. Manuf. Technol.* **2013**, *69*, 2578. [CrossRef]
45. Pleass, C.; Jothi, S. Influence of powder characteristics and additive manufacturing process parameters on the microstructure and mechanical behaviour of Inconel 625 fabricated by selective laser melting. *Addit. Manuf.* **2018**, *24*, 419–431. [CrossRef]
46. Song, B.; Dong, S.J.; Coddet, P.; Liao, H.L.; Coddet, C. Fabrication of NiCr alloy parts by selective laser melting: columnar microstructure and anisotropic mechanical behavior. *Mater. Des.* **2014**, *53*, 1–7. [CrossRef]
47. Strößner, J.; Terock, M.; Glatzel, U. Mechanical and microstructural investigation of nickel-based superalloy IN718 manufactured by selective laser melting (SLM). *Adv. Eng. Mater.* **2015**, *17*, 1099–1105. [CrossRef]
48. Saedi, S.; Turabi, A.S.; Andani, M.T.; Moghaddam, N.S.; Elahinia, M.; Karack, H.E. Texture, aging, and superelasticity of selective laser melting fabricated Ni-rich NiTi alloys. *Mater. Sci. Eng. A* **2017**, *686*, 1–10. [CrossRef]
49. Li, C.; Guo, Y.B.; Zhao, J.B. Interfacial phenomena and characteristics between the deposited material and substrate in selective laser melting Inconel 625. *J. Mater. Process. Technol.* **2017**, *243*, 269–281. [CrossRef]
50. Li, C.; White, R.; Fang, X.Y.; Weaver, M.; Guo, Y.B. Microstructure evolution characteristics of Inconel 625 alloy from selective laser melting to heat treatment. *Mater. Sci. Eng. A* **2017**, *705*, 20–31. [CrossRef]
51. Liu, Q.C.; Elambasseril, J.; Sun, S.J.; Leary, M. The Effect of manufacturing defects on the fatigue behaviour of Ti-6Al-4V specimens fabricated using selective laser melting. *Adv. Mater. Res* **2014**, *891–892*, 1519–1524. [CrossRef]
52. Qiu, C.L.; Chen, H.X.; Liu, Q.; Yue, S.; Wang, H.M. On the solidification behaviour and cracking origin of a nickel-based superalloy during selective laser melting. *Mater. Charact.* **2019**, *148*, 330–344. [CrossRef]
53. Carter, L.N.; Wang, X.; Read, N.; Khan, R.; Aristizabal, M.; Essa, K.; Attallah, M.M. Process optimisation of selective laser melting using energy density model for nickel based superalloys. *Mater. Sci. Technol.* **2016**, *32*, 657–661. [CrossRef]
54. Tascioglu, E.; Kaynak, Y.; Poyra, O.; Orhangül, A.; Ören, S. The effect of finish–milling operation on surface quality and wear resistance of Inconel 625 produced by selective laser melting additive manufacturing. In *International Conference on Advanced Surface Enhancement*; Springer: Singapore, 2019; pp. 263–272.
55. Li, S.; Wei, Q.; Shi, Y.; Chua, C.K.; Zhu, Z.; Zhang, D. Microstructure characteristics of Inconel 625 superalloy manufactured by selective laser melting. *J. Mater. Sci. Technol.* **2015**, *31*, 946–952. [CrossRef]
56. Mumtaz, K.; Hopkinson, N. Top surface and side roughness of Inconel 625 parts processed using selective laser melting. *Rapid Prototyp. J.* **2009**, *15*, 96–103. [CrossRef]
57. Witkin, D.B.; Adams, P.; Albright, T. Microstructural evolution and mechanical behavior of nickel–based superalloy 625 made by selective laser melting. In *Laser 3D Manufacturing II*; International Society for Optics and Photonics: San Francisco, CA, USA, 2015; p. 93530B.
58. Gan, Z.; Lian, Y.; Lin, S.E.; Jones, K.K.; Liu, W.K.; Wagner, G.J. Benchmark study of thermal behavior, surface topography, and dendritic microstructure in selective laser melting of Inconel 625. *Integr. Mater. Manuf. Innov.* **2019**, *8*, 178–193. [CrossRef]
59. Yang, Q.; Wu, Y.; Sha, F. Microstructure and mechanical properties of Inconel 625 alloy manufactured by selective laser melting. *Mater. Mech. Eng.* **2016**, *40*, 83–87.
60. Dinda, G.P.; Dasgupta, A.K.; Mazumder, J. Laser aided direct metal deposition of Inconel 625 superalloy: Microstructural evolution and thermal stability. *Mater. Sci. Eng. A* **2009**, *509*, 98–104. [CrossRef]
61. Wong, H.; Dawson, K.; Ravi, G.A.; Howlett, L.; Jones, R.O.; Sutcliffe, C.J. Multi-laser powder bed fusion benchmarking—Initial trials with Inconel 625. *Int. J. Adv. Manuf. Technol.* **2019**, *105*, 2891–2906. [CrossRef]

62. Poulin, J.-R.; Kreitcberg, A.; Terriault, P.; Brailovski, V. Long fatigue crack propagation behavior of laser powder bed-fused Inconel 625 with intentionally-seeded porosity. *Int. J. Fatigue* **2019**, *127*, 144–156. [CrossRef]
63. Amato, K.; Hernandez, J.; Murr, L.; Martinez, E.; Gaytan, S.; Shindo, P.; Collins, S. Comparison of microstructures and properties for a Ni–base superalloy (alloy 625) fabricated by electron beam melting. *J. Mater. Sci. Res.* **2012**, *1*, 3–41. [CrossRef]
64. Li, S. Fundamental Research on the Microstructure and Properties Evolution of Nickel-based Superalloy Fabricated by Selective Laser Melting. Ph.D. Thesis, Huazhong University of Science and Technology, Materials Processing Engineering, State Key Laboratory of Die & Mould Technology, Wuhan, China, 2017; pp. 65–66.
65. Fang, X.Y.; Li, H.Q.; Wang, M.; Li, C.; Guo, Y.B. Characterization of texture and grain boundary character distributions of selective laser melted Inconel 625 alloy. *Mater. Charact.* **2018**, *143*, 182–190. [CrossRef]
66. Kreitcberg, A.; Brailovski, V.; Turenne, S. Effect of heat treatment and hot isostatic pressing on the microstructure and mechanical properties of Inconel 625 alloy processed by laser powder bed fusion. *Mater. Sci. Eng. A* **2017**, *689*, 1–10. [CrossRef]
67. Balbaa, M.A.; Elbestawi, M.A.; McIsaac, J. An experimental investigation of surface integrity in selective laser melting of Inconel 625. *Int. J. Adv. Manuf. Technol.* **2019**, *104*, 3511–3529. [CrossRef]
68. Zhang, J.; Li, S.; Wei, Q.; Shi, Y.; Wang, L.; Guo, L. Cracking behavior and inhibiting process of Inconel 625 alloy formed by selective laser melting. *Chin. J. Rare Met.* **2015**, *39*, 961–966.
69. Vasinonta, A.; Beuth, J.; Griffith, M. Process maps for controlling residual stress and melt pool size in laser-based SFF processes. *Solid Free. Fabr. Proc.* **2000**, *8*, 200–208.
70. Leary, M.; Mazur, M.; Williams, H.; Yang, E.; Alghamdi, A.; Lozanovski, B.; Zhang, X.; Shidid, D.; Farahbod–Sternahl, L.; Witt, G.; et al. Inconel 625 lattice structures manufactured by selective laser melting (SLM): mechanical properties, deformation and failure modes. *Mater. Des.* **2018**, *157*, 179–199. [CrossRef]
71. Zhang, B.C.; Bi, G.J.; Nai, S.; Sun, C.N.; Wei, J. Microhardness and microstructure evolution of TiB2 reinforced Inconel 625/TiB2 composite produced by selective laser melting. *Opt. Laser Technol.* **2016**, *80*, 186–195. [CrossRef]
72. Marchese, G.; Colera, X.G.; Calignano, F.; Lorusso, M.; Biamino, S.; Minetola, P.; Manfredi, D. Characterization and comparison of Inconel 625 processed by selective laser melting and laser metal deposition. *Adv. Eng. Mater.* **2017**, *19*, 1600635. [CrossRef]
73. Harrison, N.J. Selective Laser Melting of Nickel Superalloys: Solidification, Microstructure and Material Response. Ph.D. Thesis, The University of Sheffield, Faculty of Engineering, School of Mechanical Engineering, Sheffield, UK, 2016; p. 203.
74. Wang, P.; Zhang, B.; Tan, C.C.; Raghavan, S.; Lim, Y.-F.; Sun, C.-N.; Wei, J.; Chi, D. Microstructural characteristics and mechanical properties of carbon nanotube reinforced Inconel 625 parts fabricated by selective laser melting. *Mater. Des.* **2016**, *112*, 290–299. [CrossRef]
75. Yadroitsev, I.; Thivillon, L.; Bertrand, P.; Smurov, I. Strategy of manufacturing components with designed internal structure by selective laser melting of metallic powder. *Appl. Surf. Sci.* **2007**, *254*, 980–983. [CrossRef]
76. Inaekyan, K.; Kreitcberg, A.; Turenne, S.; Brailovski, V. Microstructure and mechanical properties of laser powder bed-fused IN625 alloy. *Mater. Sci. Eng. A* **2019**, *768*, 138481. [CrossRef]
77. Koutiri, I.; Pessard, E.; Peyre, P.; Amlou, O.; Terris, T.D. Influence of SLM process parameters on the surface finish, porosity rate and fatigue behavior of as–built Inconel 625 parts. *J. Mater. Process. Technol.* **2018**, *255*, 536–546. [CrossRef]